Volume 1 | Number 1 | Jan 2013 | Pages 1–100

Journal of
Materials Chemistry A

Materials for energy and sustainability
www.rsc.org/materialsA

ROYAL SOCIETY OF CHEMISTRY

www.rsc.org/materialsA

Journal Name

ARTICLE

Conductive interwoven bamboo carbon fibers membrane for Li–S batteries

Xingxing Gu,[ab] Chao Lai,[a] Fei Liu,[b] Wenlong Yang,[b] Yanglong Hou,*[b] and Shanqing Zhang*[a]

Natural bamboo, as a sustainable precursor, is used to prepare porous bamboo carbon fibers (BCFs) that are subsequently interwoven into a BCF membrane (BCFM) as a captor interlayer for the lithium polysulfide intermediates between the sulfur cathode and the separator in Li–S batteries. On one hand, the interwoven BCFs offer efficient conductive networks. On the other hand, the pores of the BCFM facilitate fast mass transport of electrolyte and Li ions and accommodate severe volume changes of the sulfur cathode during charge/discharge processes. Furthermore abundant macro/micro porous structures of BCFs provide substantial adsorption capability to remarkably suppress the formation of Li_2S_2/Li_2S layer on the cathode and extend the lifetime of electrode by successfully confining sulfur within the carbon networks. Consequently, Li–S batteries with the BCFM deliver excellent electrochemical performances with a high coulombic efficiency (ca. 98%), low capacity fade at only 0.11% per cycle, and long-term cyclability over 300 cycles at a high charge/discharge rate of 1 C. This green, low cost BCFM can provide an attractive alternative for large-scale commercialization of Li–S batteries.

Introduction

Due to the rapid decline of fossil fuels and unsustainable resources such as coal, crude oil and minerals, modern society demands the development of efficient energy storages devices from naturally sustainable abundant and low cost materials such as sulfur (S) and carbon (C).

Sulfur is considered as an appealing high-capacity cathode for rechargeable lithium batteries due to its high theoretical capacity of 1672 mAh/g, high theoretical energy density of 2600 Wh/kg[1-4]. This makes the lithium-sulfur (Li–S) battery one of the most promising candidates for the next generation energy storage devices. However, the commercialization of Li–S batteries has been hampered by numerous barriers, including the low utilization of the active material, undesirable cycling stability, poor coulombic efficiency and unsatisfactory rate performance[5, 6]. It is believed that these problems are caused by factors: 1) the insulator nature of sulphur and its discharge product Li_2S_2/Li_2S[5, 6]; 2) instability of the electrode due to large volume expansion (up to 80%) of the sulfur cathode in the charge–discharge processes[7-10]; 3) the dissolution and shuttle effect of the lithium polysulfide intermediates (i.e., Li_2S_x, $4 \leq x \leq 8$) into the organic electrolyte during the charge/discharge processes[3, 5, 6].

In order to overcome these obstacles and improve the electrochemical performances of the Li–S batteries, researchers have developed various strategies, including encapsulating sulfur into conductive carbon materials[11-14], coating conductive polymer[7, 15, 16], adding metal oxides as polysulfides adsorbents[8, 17, 18] and so on. However, these approaches commonly involve the consumption and/or production of expensive, non-sustainable and toxic chemicals, sophisticated processes and high production costs. Furthermore, the resultant Li–S batteries still can't retain a good cycling performance, particularly in the cases of high charge–discharge rates. Recently, Manthiram's group proposed a new strategy that an interlayer was inserted between the cathode and the separator to tackle the severe shuttle phenomenon to enhance the cycling performance at high rate[3, 19]. Since then the application of the interlayers in Li–S batteries have received increasing attentions. A variety of materials, such as graphene[20, 21], multi-walled carbon nanotubes (MWCNTs)[3, 22], carbon black[6, 23], carbonized paper[24, 25], and metal oxides[26, 27], have been employed as the interlayers in the Li–S batteries.

The carbonaceous materials originated from biomass for production of low cost and high performance energy storage devices has been becoming more and more popular with the increased consciousness of sustainability and environment[5, 28-30]. Bamboo, as one kind of renewable biomass, widely grows in

East Asia with a fast-growing speed and short harvesting period[31-33]. To date, the bamboo chopsticks are widely used in the catering industries, i.e., a total of 24 billion pairs of bamboo chopsticks have been consumed in Japan per year[33]. However, this tremendous consumption brings about a major issue — how to re-use the discarded biomass without producing greenhouse gases has acquired increasing attentions of the researchers. Herein, we attempt to recycle the waste bamboo stick to prepare the bamboo carbon fiber membrane (BCFM) for the first time. In the conventional membrane production process, the pore of the membrane is produced via the vaporization of organic solvents. Membrane produced by vaporization of organic solvent inevitably contains some dead ends that inhibit the throughput of membrane. In strong contrast, our membrane is produced from the interwoven fibres. Dead ends will be not formed in this process, which warrantee the high throughout of electrolyte and therefore facilitate mass transportation of electrolyte. Furthermore, the robust fiber network and macro/micro pores of the BCFM can facilitate rapid the transportations of the electrons and ions as well as provide physical space for efficient confinement of sulfur[29, 30]. As shown in scheme 1, such a BCFM interlayer can facilitate the cycling performance and electrochemical performance.

Experimental

Sample preparation

Bamboo carbon fibers preparation: The bamboo carbon fibers were prepared as follows[33]: the bamboo sticks were cleaned and cut into bamboo shavings (length: ~2 cm; width: ~0.3 cm; thickness: ~0.1 cm) using a penknife. Then 2.0 g of bamboo shavings in 100 mL of 3 M KOH solution treated in a hydrothermal reactor at 150 °C for 6 hours. After being cooled to room temperature, the bamboo fibers (see Fig. S1) were collected through vacuum filtration, washed with distilled water thoroughly, dried at 60 °C in a vacuum oven, and calcined at 800 °C under Ar atmosphere for 2 h to obtain the BCFs (see Fig. S1). Subsequently, the BCFs were washed with 0.1 M HCl to remove the residual KOH and dried at 60 °C in a vacuum oven.

BCFM preparation: the BCFs were ground and then mixed with polytetrafluoroethylene (PTFE) (analytical reagent, Sigma-Aldrich) at weight ratio of 95:5 (BCFs : PTFE) using ethanol (analytical reagent, Sigma-Aldrich) as the dispersant. The pastes were rolled into films with different thickness, and then cut into disks (see Fig. S2) and dried at 60 °C in vacuum oven overnight. The thin BCFM (diameter: ~11 mm; thickness: ~0.2 mm; weight: ~1.2 mg) and thick BCFM (diameter: ~11mm; thickness: ~0.38 mm; weight: ~2.0 mg) are applied as the cathode interlayers in Li–S batteries in this study as shown in scheme. 1.
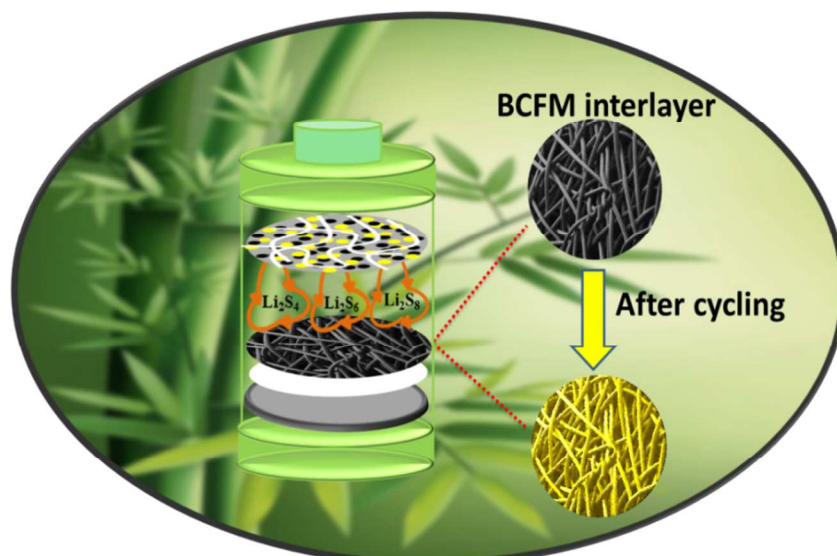
Scheme 1 A schematic configuration of the Li−S cell with a BCFM interlayer

Materials characterization

X-ray diffraction (XRD) patterns were obtained on a Philips X'Pert Pro diffractometer with Cu Kα (λ =1.5405 Å) radiation. Raman spectroscopy measurements were carried out on an HR800 Raman imaging microscope system (Horiba, France) with an excitation wavelength of 514 nm. The specific surface areas and pore volumes of BCFs were measured by the Brunauer−Emmett−Teller (BET) method using nitrogen adsorption and desorption isotherms on an ASAP 2020 system (Micromeritics, USA). The pore size distribution plot was obtained by Horvath-Kawazoe method from the adsorption branch of the N_2 adsorption/desorption isotherms. X-ray photoelectron spectroscopy (XPS) measurements were carried out on an Axis Ultra (Kratos Analytical Ltd.) imaging photoelectron spectrometer using a monochromatized Al Kα anode, and the C 1s peak at 284.8 eV was taken as an internal standard. The microstructure and morphology of all samples

were examined using a HITACHI S-4800 (Japan) scanning electron microscopy (SEM) system. The high-resolution transmission electron microscopy (HRTEM) analyses were performed using an FEI Tecnai F30 microscope (Philips-FEI, Netherlands) operated at 300 kV.

Electrochemical measurements

Pure sulfur was mixed with carbon black and PTFE in a weight ratio of 70: 20: 10 with ethanol as the dispersant. The resultant pastes were rolled into a film with a rolling rod, and cut into many pieces of wafers (see Fig. S2). Each piece of wafer was approximately 0.5 cm^2 in area and an average weight of 1.5 mg after being dried at 60 °C in a vacuum oven for 12 hours. The half-cells were assembled using a home-made module in a glove box (M-Braun, Germany) under a high pure argon atmosphere, using lithium metal as the counter electrode, polypropylene (Celgard 2300) as the separator, and 1 M lithium bis(trifluoromethanesulphonyl)imide (LiTFSI) in 1, 3-dioxolane/dimethoxy ethane (DOL/DME, 1:1, v/v) containing 0.1 M LiNO$_3$ as the electrolyte. The calculation of the specific capacity was based on the mass of the sulfur in the electrode. A LAND CT-2001A instrument (Wuhan, China) was used to test the charge and discharge performances of the half-cells, of which the potential is ranged from 1.5 to 3.0 V at room temperature. The cyclic voltammetry (CV) (scan rate: 0.1 mV/s, potential: 1.5 V−3 V) and electrochemical impedance spectroscopy (EIS) (frequency: 100 kHz−10 mHz) were carried on a CHI 660D electrochemical workstation (CHI Instrument, Shanghai, China).

Results and discussion

It is established that bamboo is mainly made up of oriented cellulose fibers embedded in a ligneous matrix[33]. During the hydrothermal process, the lignin part between adjacent bamboo fibers are dissolved into the KOH solution under the hydrothermal reaction conditions, while the tubular cellulose fibers have been separated and retained[33]. XPS was employed to investigate the surface chemical composition of nature bamboo stick, bamboo fibers and bamboo carbon. Fig. 1 displays the XPS survey spectra and Table 1 lists the surface composition of the main elements of these three samples. The XPS analyses suggest that the bamboo stick, in addition to contains common elements such as C, H, O, N, F, in plant-based precursors[33, 34], but also containing ca. 1.96 wt% impurities (e.g., Si, Ca). Other potential impurities (e.g. P, K, Mg) were below the detection limits of XPS analysis[34]. N element may mainly exist in the form of lignin as well as other soluble inorganic and inorganic salts are removed by dissolving in the concentrated KOH solution. As a result, the bamboo sticks are turned into light-yellow cotton-like loose fibers (see Fig. S1) without detectable N. Subsequently, bamboo fibers are carbonized to bamboo carbon fibers (BCFs) (see Fig. S1). As shown in Table 1, the oxygen content of BCFs declines dramatically to 5.56 wt% from 34.71% of the bamboo fiber, while carbon content increase to 93.1% from 63.7% of the bamboo fiber, which is mainly due to the decomposition of

C=O bond in the inert atmosphere during the annealing process. The high carbon content in BCFs benefits electrical conductivity and chemical stability and therefore furthers the electrochemical performance of Li−S batteries.

Table 1 chemical composition of bamboo stick, bamboo fibers and bamboo carbon via XPS surface analysis.

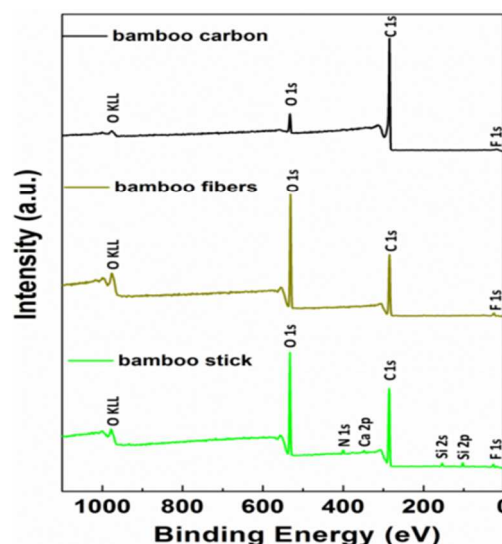| Samples	Chemical composition			
	C (wt%)	O (wt%)	F (wt%)	N (wt%)
Bamboo stick	68.55	26.50	1.47	1.52
Bamboo fibers	63.73	34.71	1.56	—
Bamboo carbon	93.08	5.56	1.36	—

Fig. 1 XPS survey spectra of bamboo stick, bamboo fibers and bamboo carbon.

The micro morphology of bamboo fibers and bamboo carbon can be observed under SEM in Fig. 2. As shown in Fig. 2a, after hydrothermal process, the bamboo sample illustrates cotton-like micro fiber structure. Fig. 2b shows that the bamboo carbon retains the fiber morphology after bamboo fibers annealed. And from the Fig. 2c, the rough surface with some small gaps and macropores of BCFs are observed; and hollow structure of BCFs is evidenced in the inset of Fig. 2c. These unique structures are advantageous to electrolyte infiltrating, trapping polysulfides and accommodating the severe volume change of the sulfur cathode during charge–discharge processes[3]. The BCFs interacting with each other can readily form a 3D structure when they form a film with the binder, which not only facilitates electron transfer, but also helps confine the active materials in a reusable region[3]. In addition, we can observe large amount of black dots with the diameter size of <1 nm in Fig. 2d, which shows that the BCFs consist of substantial amount of micropores[2, 35, 36], which agrees well with

the undermentioned N_2 adsorption/desorption results. The structure of the hollow tubes, macropores and micropores is very likely generated in the presence of residual KOH on the bamboo fibers in the course of high temperature carbonization process.
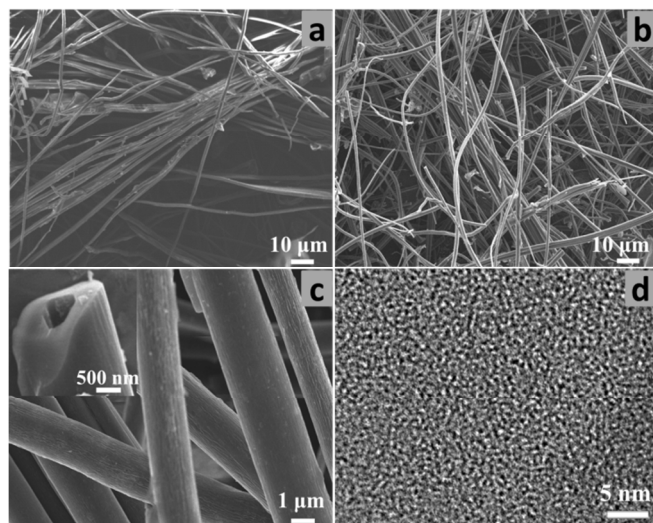

Fig. 2 SEM images of (a) bamboo fibers, (b,c) BCFs, and (d)TEM image of BCFs.

The N_2 adsorption/desorption was employed to characterize the textural properties of the BCFs. Fig. 3 illustrates the isotherm plot and pore size distribution of the BCFs. It is clearly observed that the BCFs have a narrow micropore size distribution, mainly in the range of ca. 0.75 and 1.58 nm, respectively, which is consistent with the TEM observations. A type I isotherm (a Langmuir-type isotherm) also indicates the characteristic microporous structure of the BCFs[2, 33]. The BET areas and micropore volumes of the BCFs are 776.07 m²/g and 0.33 cm³/g, respectively. The high specific surface area and pore volume can provide more reactive sites that are beneficial to the utilization of active materials sulfur[2, 9] because the micropores can not only supply facile transport channels for Li-ions[37], but also efficiently retain the polysulfides intermediates in the cathodic chamber to reduce the loss of the active materials and prevent the polysulfides shuttle to the anodic compartment[2, 9, 19].
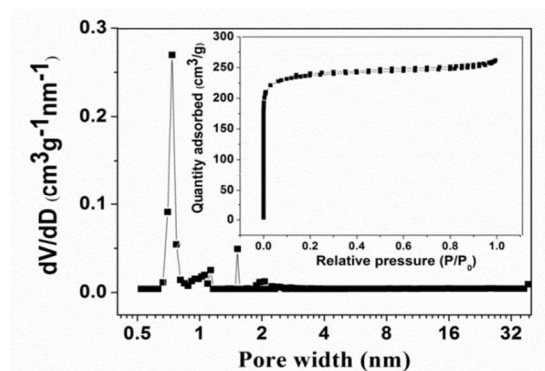

Fig. 3 Isotherm plot and pore size distribution of the BCFs.

The XRD pattern (Fig. 4a) and Raman spectrum (Fig. 4b) are used to characterize the graphitization of BCFs. The two broad diffraction peaks present in the XRD pattern are assigned to the (002) and (100) facets of the hexagonal carbon, indicating the graphite domain/crystal size is not predominant as in previous literature[33]. The Raman spectrum shows two fingerprint peaks at 1358 cm^{-1} and 1590 cm^{-1} that correspond to a disorder-induced D band and an in-plane vibrational G band, respectively[5, 33]. The peak height ratio of I_D/I_G is 0.93, indicating the partial graphitization of BCFs in the pyrolysis process at 800 ˚C, which is actually beneficial to the electronic conductivity of BCFs[5].
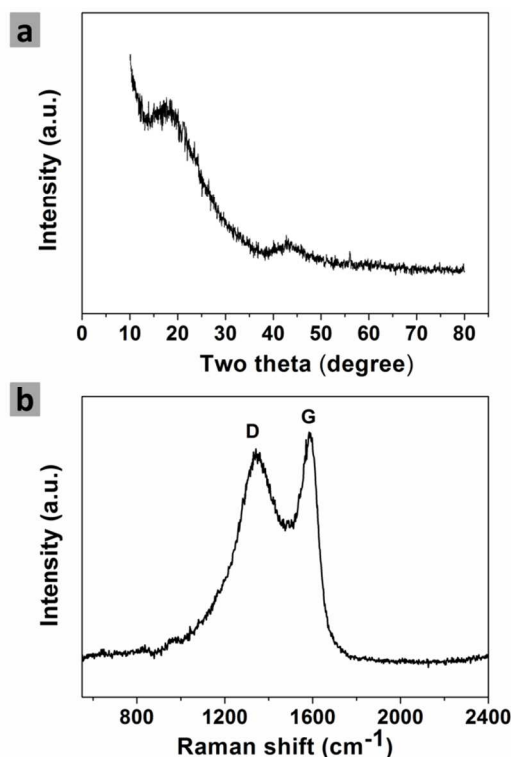

Fig. 4 (a) XRD diffractogram and (b) Raman spectrum of the BCFs.

The cyclic voltammetry (CV) curves of the Li–S batteries with and without BCFM interlayer are illustrated in Fig. 5a and 5b, respectively. In the cathodic scan, two remarkable reduction peaks are corresponding to the two discharge plateaus in Fig. 5c and 5d. The peak at the higher voltage corresponds to the conversion of element sulphur to soluble lithium polysulfides (Li_2S_x, $4 \leq x \leq 8$), while the reduction peak at the lower voltage corresponds to the reduction of soluble polysulfides to insoluble Li_2S_2 and Li_2S[5, 29]. In the subsequent anodic scan, only one oxidation peak is observed in the cell with the BCFM interlayer, corresponding to the oxidation of Li_2S_2 or Li_2S to the soluble lithium polysulfides[5]. However, the cell without BCFM interlayer shows that two typical oxidation peaks overlap and form one large peak at ca. 2.60 V (Fig. 5b) during the first anodic scan. This overlap may be due to the higher overpotential, leading the conversion of Li_2S to Li_2S_x and further polarization, which is not observed for the cell with

BCFM [29, 38]. In addition, the cathodic and anodic peaks of CV curves for the cell with BCFM interlayer are overlapped in terms of peak currents and peak positions in a larger extend, again suggesting smaller polarization and better reversibility[39] than the cell without the BCFM interlayer.

Typical voltage-capacity profiles of the cells with and without BCFM interlayer at 1 C are illustrated in Fig. 5c and 5d, respectively. These discharge curves exhibit two typical plateaus as observed for the Li–S batteries, which is assigned to a two-step reaction of sulfur with lithium during the discharge process. This phenomenon coincides with the observation in the CV measurements. In addition, the cell with the BCFM interlayer shows initial capacity of 907.8 mAh/g and maintains a reversible capacity of 605.7 mAh/g after 300 cycles at a high rate of 1 C, indicating that the BCFM interlayer can effectively retain a high utilization of active sulfur and substantially suppress the polysulfides shuttling to lithium anode[5]. It can be observed that the electrode has been so stable that the 100th and 300th discharge profiles are nearly overlapping with each other, implying excellent cyclability brought by the BCFM interlayer[5].

network can boost the electron transport, enhance the cathode conductivity and improve the active material utilization[3, 25, 29]; 2) the porous structures not only ensure the electrolyte immersion[25], but also effectively adsorb the polysulfides and decrease the dissolution and shuttling[3, 5, 19, 29]; 3) the conductive pores of BCFM provide effective channels for rapid mass transport and simultaneously provide physical space to tolerate severe volume variation of the sulfur cathode during the cycling processes[3, 22]; 4) the BCFM interlayer itself serves as the physical barrier to trap the polysulfides and prevent shuttling[20, 22].

Table 2 Electrochemical performance of Li-S cells basing on different porous biochar carbon

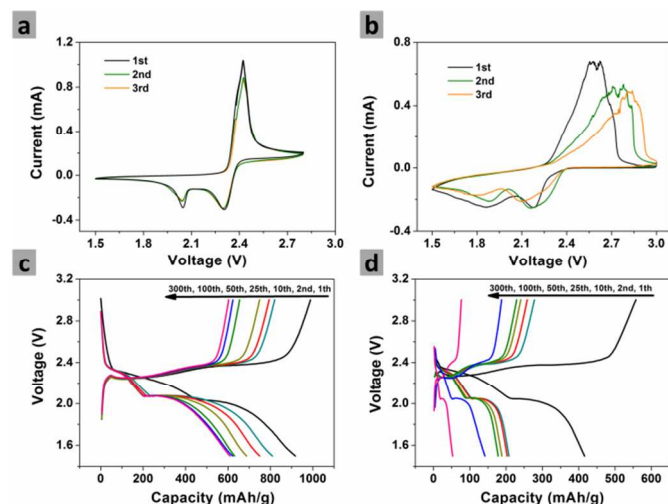| Biochar interlayer type	Initial capacity (mAh/g)	Cycle capacity (mAh/g)	Rate (C)	S (%)	Ref.
Cassava derived carbon	1318	811 (100th)	0.5	60	5
Fungi carbon	~970	650 (100th)	0.5	60	28
Carbonized eggshell membrane	1327	~1000 (100th)	0.1	–	29
Leaf carbon	~1000	829 (100th)	0.5	70	30
BCFM	907	605 (300th)	1	70	This work

Fig. 5 Cyclic voltammetry (CV) curves of the Li–S batteries (a) with 1.2 mg interlayer and (b) without interlayer at 0.1 mV/s, voltage capacity profiles of the Li–S batteries (c) with 1.2 mg interlayer and (d) without interlayer at 1 C.

The cycling performances of the cells with and without BCFM interlayer at a rate of 1 C between 1.5 V and 3 V are displayed in Fig. 6a. It is evident that with the BCFM interlayer, the reversible capacity has been enhanced regardless of thickness. In particular, the reversible capacity of the cell with the thin interlayer (1.2 mg) is 605.7 mAh/g with high coulombic efficiency of ca. 98% and low capacity fade of ca. 0.11% per cycle after 300 cycles. And we have compared this performance to other biochar interlayer in Li–S batteries as shown in table 2, and found the Li–S batteries with BCFM interlayer showed better performances regarding to the high rate and long cycle when compared to previous reported biochar interlayer. The significant increase on cycling performance may be attributed to the advantages provided by the BCFs: 1) the 3D fiber
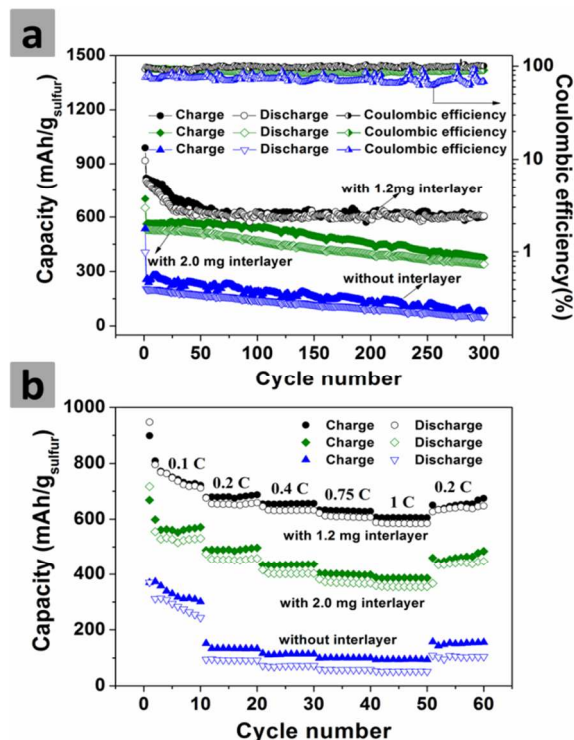

Fig. 6 (a) Cycle life of the cells with and without interlayer at 1 C and (b) rate capability of the cells with and without interlayer.

Furthermore, the rate capability performances of the cells with and without BCFM interlayer are observed in Fig. 6b. It is

clearly observed the cells with the BCFM interlayer exhibit better performance at different current densities than the one without interlayer. In particular the cell with the thin interlayer shows the best rate capability—during the first 10 cycles, the discharge capacity fade gradually at 0.1 C and retained the capacity of 711 mAh/g. At middle rate of 0.2 C and 0.4 C, the capacity of 659 mAh/g and 632 mAh/g can be delivered respectively. Further cycling at high rate of 0.75 C and 1 C, a reversible capacity of about 617 mAh/g (70% of initial capacity) and 588 mAh/g (65% of initial capacity) is reached, respectively. When the rate is switched to 0.2 C again, a reversible capacity of approximately 650 mAh/g can still be restored, suggesting excellent redox stability of the cell with BCFM interlayer[2, 5]. In contrast, the cell without the interlayer shows fast capacity fading at the same increasing charge–discharge rate. The excellent rate performance of the cell with BCFM interlayer can be credited to the good conductivity of BCFM, abundant microporous structure of BCFs, which can strongly trap the polysulfides and unique interwoven 3D structure of BCFM that can transfer lithium ion to active material easily and quickly[5, 40].

More interestingly, herein, the thin BCFM interlayer sample shows significantly better cycling performance (Fig. 6a) and rate capability (Fig. 6b) than the thick interlayer sample. In this circumstance, the thickness of the interlayer plays an important role in mass transports of the electrolyte and ions as well as the electronic conductivity. Apparently, thinner layer facilitates the infiltration of the electrolyte and the passage of the electron and the ions. This can be somehow suggested by similar stability and the relatively consistent difference between the thin interlayer sample and the thick one in rate capability in Fig. 6. The following EIS analysis will further support this argument by calculation charge-transfer resistance (R_{ct}), values of different thickness interlayer in Figure 7 and Table 3.

Fig. 7a and 7b illustrate the EIS and the equivalent circuit models of the cells before discharge and after discharging 100 cycles, respectively, which are beneficial to better understand the improved electrochemical performances with the use of a BCFM interlayer. Before discharging, it can be observed the Nyquist plots of all the cells are composed of a medium-to-high frequency semicircle and a long inclined line (Warburg impedance) in the low frequency region. The high-frequency intercept on the real axis represents the ohmic resistance (R_e) of the cell, including the electrolyte and electrode resistances. The semicircle at high- to medium-frequency is resulted from the interface charge-transfer resistance (R_{ct}), and the inclined line at the low-frequency region corresponds to Warburg impedance (W_o). However, after 100 cycles two obvious semicircles can be observed from the Nyquist plot of the cell without the BCFM interlayer. The semicircle in the high-frequency region reflects the interfacial charge transfer process[2, 10], and the semicircle in the medium-frequency range is related to the resistance of the solid-electrolyte-interface (SEI) film[2, 10], which is contributed by the Li_2S (or Li_2S_2) layers on the surface of the electrode[2, 10]. The fitted R_e, R_s, R_{ct} values of the cells according to the equivalent circuit are shown in Table 3. It is found that the R_{ct}

of the cell without the BCFM interlayer is much higher than that of the cells with the BCFM interlayer before discharge, which can be ascribed to the enhanced conductivity after inserting the BCFM in the cells. And the R_{ct} of the cell with the 1.2 mg interlayer (the thin interlayer sample) is even smaller than the thick sample. This refers to the aforementioned reasons, i.e., the thinner film is more favourable for Li ions mass transport and electrons transfer. After 100 cycles, the R_{ct} values of all the cells decrease remarkably in comparison with that at the beginning, which may be due to the infiltration of the electrolyte and chemical activation process for the dissolution and redistribution of the active materials[26]. Furthermore, the decrease R_{ct} values indicate the formation of the SEI film on the surface of the electrode makes the Li ions transportation easier[2, 41]. As to the R_s, it is clearly observed that the values of the cells with the BCFM interlayer are far smaller than those of the cells without the BCFM interlayer. Especially, the cell with the thick interlayer has smaller R_s value, further demonstrating that the BCFM interlayer could efficiently prevent the polysulfides from shuttling to the anode and growing the Li_2S_2/Li_2S film.
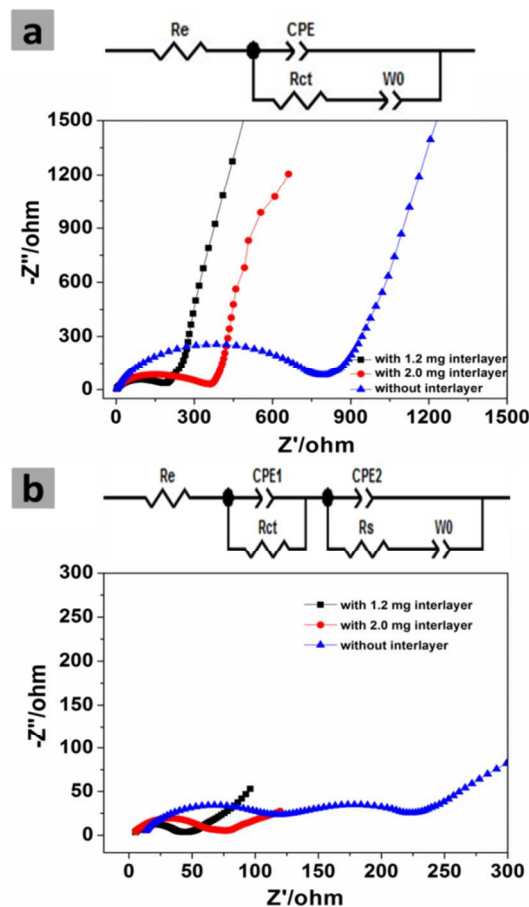

Fig. 7 The Nyquist plots (a) before discharge and (b) after 100 cycles of the Li–S cells with and without BCFs interlayer and equivalent circuit models.

Table 3 Impedance parameters calculated according to the equivalent circuits

Sample name	Cycle number	Resistance		
		R_e (Ω)	R_s (Ω)	R_{ct} (Ω)
Without BCFs interlayer	Before cycling	1.01	—	824.40
	100th cycles	9.74	78.59	173.4
With 2.0 mg BCFs interlayer	Before cycling	1.15	—	377.10
	100th cycles	2.82	8.36	58.07
With 1.2 mg interlayer	Before cycling	0.89	—	195.5
	100th cycles	3.30	30.16	19.56

Conclusions

The BCFM derived from natural bamboo have been successfully employed as the interlayer in Li–S batteries. Thin BCFM interlayer bestows Li–S batteries excellent long-term cycle stability (only 0.11% capacity fade per cycle), high coulombic efficiency (~ 98%) and superior rate capability even when the sulfur content is as high as 70% in the electrode. The exceptional performance can be attributed to the resultant conductive fiber networks, providing conductive skeletons for the deposition of sulfur, pores of BCFM to facilitate swift mass transport of electrolyte and Li ions and to tolerate dramatic volume changes during charge–discharge processes, as well as the ample macro/micropore structures of BCFM for trapping the polysulfides. A thin BCFM layer not only adequately retains polysulfides intermediates within the interlayer and supresses the shuttling effect, but also facilitates conduction of electrons and mass transport of Li ions by providing more efficient electrolyte infiltration and shortening electron transfer distance. With additional merits of being simple, up-scalable, sustainable and low cost BCFM can be one of the promising alternatives to the mass manufacturing of Li–S batteries.

Acknowledgements

Notes and references
[a] Centre for Clean Environment and Energy, Environmental Futures Institute, Griffith School of Environment, Gold Coast Campus, Griffith University QLD 4222, Australia. Fax: 61-755047588; Tel: 61-7-55528155; E-mail: s.zhang@griffith.edu.au
[b] Department of Materials Science and Engineering, College of Engineering, Peking University, Beijing 100871, China. E-mail: hou@pku.edu.cn

1. C. Zu, Y. S. Su, Y. Fu and A. Manthiram, *Phys. Chem. Chem. Phys.*, 2013, **15**, 2291–2297.
2. X. Gu, Y. Wang, C. Lai, J. Qiu, S. Li, Y. Hou, W. Martens, N. Mahmood and S. Zhang, *Nano Res.*, 2014, DOI: 10.1007/s12274-12014-10601-12271.
3. Y. S. Su and A. Manthiram, *Chem. Commun.*, 2012, **48**, 8817–8819.
4. N. Mahmood, C. Zhang, H. Yin and Y. Hou, *J. Mater. Chem. A*, 2014, **2**, 15–32.
5. F. R. Qin, K. Zhang, J. Fang, Y. Q. Lai, Q. Li, Z. A. Zhang and J. Li, *New J. Chem.*, 2014, **38**, 4549–4554.
6. S. H. Chung and A. Manthiram, *Adv. Funct. Mater.*, 2014, **24**, 5299–5306.
7. G. Q. Ma, Z. Y. Wen, J. Jin, Y. Lu, X. W. Wu, M. F. Wu and C. H. Chen, *J. Mater. Chem. A*, 2014, **2**, 10350–10354.
8. Y. G. Zhang, Y. Zhao, A. Yermukhambetova, Z. Bakenov and P. Chen, *J. Mater. Chem. A*, 2013, **1**, 295–301.
9. S. Zhao, C. Li, W. Wang, H. Zhang, M. Gao, X. Xiong, A. Wang, K. Yuan, Y. Huang and F. Wang, *J. Mater. Chem. A*, 2013, **1**, 3334–3339.
10. W. G. Wang, X. Wang, L. Y. Tian, Y. L. Wang and S. H. Ye, *J. Mater. Chem. A*, 2014, **2**, 4316–4323.
11. L. Wang, Y. Zhao, M. L. Thomas and H. R. Byon, *Adv. Funct. Mater.*, 2014, **24**, 2248–2252.
12. X. Yang, L. Zhang, F. Zhang, Y. Huang and Y. Chen, *ACS Nano*, 2014, **8**, 5208–5215.
13. Z. Li, Y. Jiang, L. Yuan, Z. Yi, C. Wu, Y. Liu, P. Strasser and Y. Huang, *ACS Nano*, 2014, **8**, 9295–9303.
14. C. Zhao, L. Liu, H. Zhao, A. Krall, Z. Wen, J. Chen, P. Hurley, J. Jiang and Y. Li, *Nanoscale*, 2014, **6**, 882–888.
15. J. Wang, L. Yin, H. Jia, H. Yu, Y. He, J. Yang and C. W. Monroe, *ChemSusChem*, 2014, **7**, 563–569.
16. W. Y. Li, G. Y. Zheng, Y. Yang, Z. W. Seh, N. Liu and Y. Cui, *P.Nat. Acad. Sci.U. S. A.*, 2013, **110**, 7148–7153.
17. Z. Liang, G. Y. Zheng, W. Y. Li, Z. W. Seh, H. B. Yao, K. Yan, D. S. Kong and Y. Cui, *ACS Nano*, 2014, **8**, 5249–5256.
18. Z. W. Seh, W. Li, J. J. Cha, G. Zheng, Y. Yang, M. T. McDowell, P. C. Hsu and Y. Cui, *Nat. Commun.*, 2013, **4**, 1331–1336.
19. Y. S. Su and A. Manthiram, *Nat. Commun.*, 2012, **3**, 1166–1171.
20. G. Zhou, S. Pei, L. Li, D. W. Wang, S. Wang, K. Huang, L. C. Yin, F. Li and H. M. Cheng, *Adv. Mater.*, 2014, **26**, 625–631.
21. X. Wang, Z. Wang and L. Chen, *J. Power Sources*, 2013, **242**, 65–69.
22. S.-H. Chung and A. Manthiram, *J. Phys. Chem. Lett.*, 2014, **5**, 1978–1983.
23. H. Yao, K. Yan, W. Li, G. Zheng, D. Kong, Z. W. Seh, V. K. Narasimhan, Z. Liang and Y. Cui, *Energy Environ. Sci.*, 2014, **7**, 3381–3390.

24. K. Zhang, Q. Li, L. Zhang, J. Fang, J. Li, F. Qin, Z. Zhang and Y. Lai, *Mater. Lett.*, 2014, **121**, 198–201.

25. S. H. Chung and A. Manthiram, *Chem. Commun.*, 2014, **50**, 4184–4187.

26. Z. Zhang, Y. Lai, Z. Zhang, K. Zhang and J. Li, *Electrochim. Acta*, 2014, **129**, 55–61.

27. W. Li, J. Hicks-Garner, J. Wang, J. Liu, A. F. Gross, E. Sherman, J. Graetz, J. J. Vajo and P. Liu, *Chem. Mater.*, 2014, **26**, 3403–3410.

28. L. Zhang, Y. Wang, B. Peng, W. Yu, H. Wang, T. Wang, B. Deng, L. Chai, K. Zhang and J. Wang, *Green Chem.*, 2014, **16**, 3926–3934.

29. S. H. Chung and A. Manthiram, *Adv. Mater.*, 2014, **26**, 1360–1365.

30. S. H. Chung and A. Manthiram, *ChemSusChem*, 2014, **7**, 1655–1661.

31. Y. Zhao, Y. Huang, Q. Wang, W. Zhang, K. Wang and M. Zong, *J. Appl. Electrochem.*, 2013, **43**, 1243-1248.

32. B. H. Hameed, A. T. Din and A. L. Ahmad, *J. Hazard. Mater.*, 2007, **141**, 819–825.

33. J. Jiang, J. H. Zhu, W. Ai, Z. X. Fan, X. N. Shen, C. J. Zou, J. P. Liu, H. Zhang and T. Yu, *Energy Environ. Sci.*, 2014, **7**, 2670–2679.

34. J. Ding, H. Wang, Z. Li, K. Cui, D. Karpuzov, X. Tan, A. Kohandehghan and D. Mitlin, *Energy Environ. Sci.*, 2015, DOI: 10.1039/c1034ee02986k.

35. B. Zhang, X. Qin, G. R. Li and X. P. Gao, *Energy Environ. Sci.*, 2010, **3**, 1531–1537.

36. D. W. Wang, G. Zhou, F. Li, K. H. Wu, G. Q. Lu, H. M. Cheng and I. R. Gentle, *Phys Chem Chem Phys*, 2012.

37. L. Zhou, X. Lin, T. Huang and A. Yu, *Electrochim. Acta*, 2014, **116**, 210–216.

38. D. Li, F. Han, S. Wang, F. Cheng, Q. Sun and W. C. Li, *ACS Appl. Mater. Interfaces*, 2013, **5**, 2208–2213.

39. K. Zhang, F. Qin, J. Fang, Q. Li, M. Jia, Y. Lai, Z. Zhang and J. Li, *J. Solid State Electrochem.*, 2014, **18**, 1025–1029.

40. J. Song, Z. Yu, T. Xu, S. Chen, H. Sohn, M. Regula and D. Wang, *J. Mater. Chem. A*, 2014, **2**, 8623–8627.

41. B. Ding, C. Yuan, L. Shen, G. Xu, P. Nie and X. Zhang, *Chem. Eur. J.*, 2013, **19**, 1013–1019.